



HAL
open science

A practical approach to the evaluation of local urban overheating– A coastal city case-study

S. Martinez, A. Machard, A. Pellegrino, K. Touili, L. Servant, Emmanuel Bozonnet

► **To cite this version:**

S. Martinez, A. Machard, A. Pellegrino, K. Touili, L. Servant, et al.. A practical approach to the evaluation of local urban overheating– A coastal city case-study. *Energy and Buildings*, 2021, 253, pp.111522. 10.1016/j.enbuild.2021.111522 . hal-03374590

HAL Id: hal-03374590

<https://hal.science/hal-03374590v1>

Submitted on 16 Oct 2023

HAL is a multi-disciplinary open access archive for the deposit and dissemination of scientific research documents, whether they are published or not. The documents may come from teaching and research institutions in France or abroad, or from public or private research centers.

L'archive ouverte pluridisciplinaire **HAL**, est destinée au dépôt et à la diffusion de documents scientifiques de niveau recherche, publiés ou non, émanant des établissements d'enseignement et de recherche français ou étrangers, des laboratoires publics ou privés.



Distributed under a Creative Commons Attribution - NonCommercial 4.0 International License

1 A practical approach to the evaluation of 2 local urban overheating– a coastal city 3 case-study

4 S. Martinez^{1,2}, A. Machard^{1,2}, A. Pellegrino^{1,3}, K. Touili^{1,2}, L. Servant^{1,2}, E. Bozonnet^{1,2}

5 ¹ LaSIE UMR CNRS 7356, La Rochelle Université, France

6 ² IRSTV FR CNRS 2488, France

7 ³ Politecnico di Bari, 70125 Bari, Italy

8 **Abstract**

9 In response to urbanization and global warming, which amplify heatwave effects and might
10 lead to urban heat stress, this paper proposes a practical approach to characterize the local
11 microclimate at the neighborhood scale. In this approach, the local urban climate is described
12 using suitable indicators, to support the ecodistrict design process or refurbishment.
13 Experimental and numerical results illustrate the approach in a case study of a French coastal
14 city, La Rochelle. In the first step, we set up urban and rural weather stations to characterize
15 the local urban climate over a summer period and to identify local temperature differences.
16 The measurements highlighted a daytime urban cooling effect due to the local sea breeze.
17 While the Urban Weather Generator (UWG) simulation tool used for this study does not
18 capture coastal effects, the results were consistent with the urban heat island (UHI)
19 measurements. We proposed two indicators to quantify the local climate modifications: local
20 UHI and overheating intensity. The parameters of the adaptation strategies were assessed
21 through a sensitivity analysis for these two indicators. For this case-study, we identified
22 vegetation cover, building height and road albedo as key parameters that can be used to
23 mitigate local overheating.

24 **1 Introduction**

25 In recent decades, the expansion of cities and environmental constraints [1] have resulted in
26 increasing challenges for urban planning, district renovation and building energy design.
27 Urban heat islands (UHI) are closely tied to the complex interactions between the urban
28 canopy, buildings (envelope and system waste heat), and the occupants [2,3]. In this context,
29 and to adapt to increasing temperatures due to climate change, the decision process requires
30 practical quantitative tools, and indicators to compare urban strategies and building design
31 adaptations. In this paper, we combined an experimental and numerical approach to propose
32 easy to interpret quantitative indicators. The results can be used to adapt the urban fabric to
33 future UHIs and future urban heatwaves. Indeed, the occurrence of heatwaves will increase
34 during the 21st century, and studies have shown that the UHI effect is amplified during hot
35 days and nights in dense cities [4,5]. Our approach is illustrated through a case study of a
36 coastal city (La Rochelle, France), which shows similarities with other coastal studies [6–8].
37 Indeed, under some conditions, the sea breeze may attenuate high daytime temperatures in
38 summer.

39 On hot days, in the urban context, critical periods of thermal discomfort [9,10] or thermal
40 stress [11] may occur. During the 2003 European heatwave [12], the UHI amplified the
41 intense exposure to the heatwave and led to increased mortality, especially among vulnerable
42 people. Seventy thousand deaths were correlated with the heatwave in Europe, and 15,000 in
43 France, where the highest excessive mortality rate was recorded in Paris [13]. Laaidi *et al.*
44 [14] showed that abnormally elevated night temperatures (26 °C on the warmest day of the
45 heatwave at 6 am in Paris) were due to the UHI, and had a strong impact on the health of
46 occupants in buildings. Old residential free-floating Parisian buildings are not adapted to heat,
47 and the reduced cooling effect of the urban fabric at night could explain these elevated
48 nighttime temperatures. In a recent study, an ecodistrict (i.e., an urban area with a reduced

49 carbon footprint and a sustainable design [15,16]) in Paris was modelled under a future
50 intense heatwave around the mid-century, and the results indicated that the urban
51 neighborhood would be subject to heat stress [17]. This reinforces the need to adapt the urban
52 fabric to climate change and implement effective mitigation strategies.

53 In this study, we focused on both exposure to overheating and microclimate modification due
54 to the local UHI. Exposure to overheating (defined in section 2.4.1) is specifically related to
55 summer thermal discomfort and potential heat stress within inhabited spaces. Although the
56 proposed indicators are based on common UHI and overheating definitions, this approach
57 quantifies the exposure in more detail, with two time-integrated quantitative indicators that
58 account for both exposure duration and intensity. Unlike purely numerical or spatially
59 averaged studies, our aim was to highlight the practical benefits and limitations of this
60 approach, based on the very local differences that can be captured experimentally by these
61 indicators, so that they can be used in adaptation strategy simulation and the decision-making
62 process.

63 On the one hand, we installed two urban weather stations within a specific local climate zone
64 (LCZ) [18] to highlight and quantify very local urban effects, since urban simulation tools
65 usually take into account the spatially averaged local climate (LCZ scale). Our analysis is
66 specifically supported by data recorded during a 10-day heatwave.

67 On the other hand, we used the spatially broader modelling approach with the numerical
68 Urban Weather Generator (UWG) model [19,20]. This approach is useful for experimenting
69 with various strategies to mitigate overheating, and with future weather conditions. Recent
70 studies using this model [21–25] demonstrated its potential to assess UHI, thermal discomfort
71 and health issues [26]. The neighborhood architecture may also benefit from this approach,
72 which takes into consideration different urban contexts using a modified weather file [27].

73 The UHI parameters are well-known [28–31], and we analyzed the improvement in radiative
74 properties such as increased albedo (e.g., cool roofs) and the implementation of evaporative
75 cooling (e.g., green roofs) to decrease solar heat gain on the building fabric. Susca *et al.* [32]
76 reported a 2°C difference between sparse and well-vegetated areas in New-York. Bonafoni *et*
77 *al.* [33] and Taha *et al.* [34], investigated the benefits of increased albedo on urban climate
78 and air-conditioning cooling loads. In Montreal [35], cool roofs on commercial buildings
79 could save up to 11% of cooling energy consumption. Various other advanced techniques are
80 under development to mitigate urban heat with surface modifications [36,37].

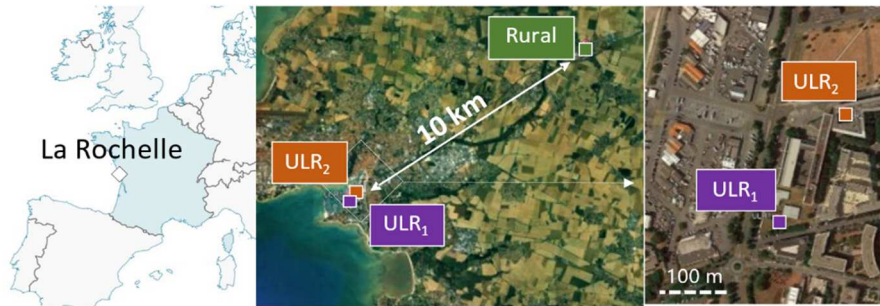
81 Through a sensitivity analysis, we analyzed the potential of these passive cooling solutions to
82 mitigate urban heat and summer overheating. For this purpose, we used the defined
83 quantitative indicators as objective functions. This method can be applied to other cities,
84 which might identify different key solutions, depending on the location. This method is
85 therefore positioned upstream of the decision-making process, and could be useful for the
86 implementation of strategies at the building and the urban area design stage, and in identifying
87 the main parameters responsible for urban overheating that could then be adjusted to achieve
88 better climate adaptation.

89 **2 Methodology**

90 2.1 Case study and methodology overview

91 The neighborhood studied is located in La Rochelle, a city on the southwest coast of France.
92 A total of three weather stations were installed. The two urban stations (ULR₁ and ULR₂)
93 were set up in the university urban neighborhood located very close to the sea (500 m), and
94 the rural station is about 10 km inland (Figure 1). Several studies suggest methods and
95 guidelines to properly install and analyze data in an urban area [38–40] such as the
96 positioning of the reference station, different methods to calculate UHI, and in particular the
97 positioning of the weather stations. The two weather stations were installed close to each

98 other (approximately 200 m) to (i) estimate local overheating and UHI, and (ii) highlight the
 99 local differences due to urban heterogeneity within the same LCZ zone.



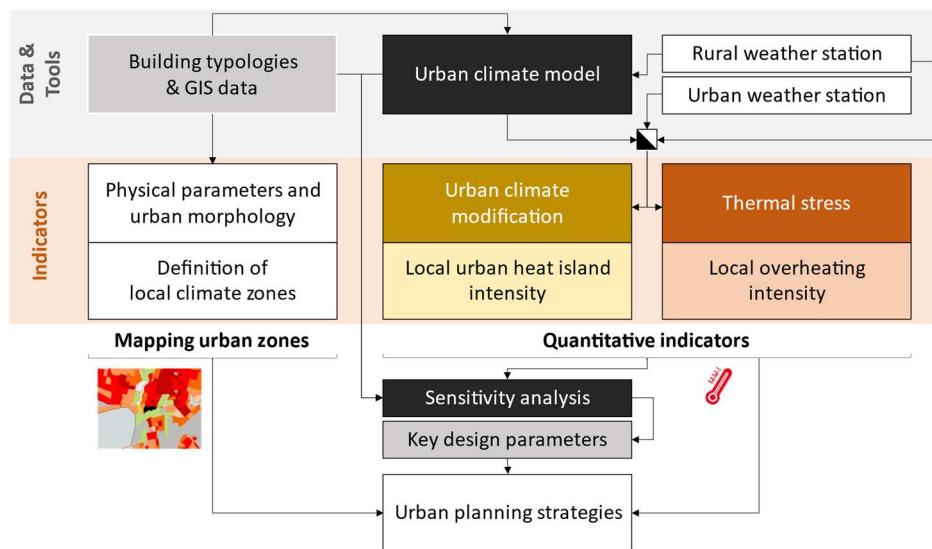
100

101

Figure 1: La Rochelle case study and weather station location

102 According to the Köppen classification [41], La Rochelle (latitude 46°2' North, longitude
 103 1°1' West) is considered a temperate oceanic climate. Even though the two urban weather
 104 stations are located in the same neighborhood, they have different surroundings. The ULR₁
 105 station was set up between buildings (dense urban context), while the ULR₂ station is in a
 106 clear field with few nearby obstacles. The period under study was a 10-day heatwave that
 107 occurred between the 20th and 30th July in the summer of 2019.

108 The proposed methodology is illustrated in Figure 2.



109

110

Figure 2: Overview of the proposed methodology

111 The methodology used in this research can be split into four parts: (i) Information on building
112 typologies and GIS data was collected for two reasons: First, to map the urban area into
113 LCZs, which are of interest to urban planners in understanding UHI risk and hot spots [42–
114 44]. They are then used as input data for the urban climate model (UWG); (ii) The urban
115 model is used to complement the meteorological stations (rural and urban) in order to
116 understand and analyze the change in the local climate in the city; (iii) In order to facilitate the
117 analysis of the data, two quantitative indicators were defined and calculated using the above.
118 The first indicator quantifies the intensity of the local urban heat island, which is related to
119 urban climate change, while the second calculates the intensity of local overheating, which
120 provides information on outdoor heat stress during heatwaves; (iv) Finally, the urban climate
121 model was used to perform a sensitivity analysis of the different design parameters during
122 urban planning, to determine the main mitigation and adaptation strategies for the coastal city
123 under study. The overall goal was that the practical indicators enable the stakeholders to
124 address overheating issues in a holistic approach that takes into account the related health
125 impacts, energy poverty and social disparity in the population.

126 2.2 Mapping urban zones

127 Stewart and Oke [18] defined the LCZ classification from urban parameters. These LCZ
128 parameters include the urban morphology and thermophysical characteristics of urban zones.

129 Long *et al.* [45] classified the LCZ for 42 French urban areas and highlighted a significant
130 link to UHI intensity, defined here as the temperature difference between urbanized and non-
131 urbanized temperature for the same location. These results were obtained from numerical
132 simulations at a spatial resolution of 250 m using the Town Energy Balance (TEB) model
133 coupled to the Méso-NH atmospheric model. In the MUSTARDijon project [46], the
134 reliability of this LCZ classification was experimentally studied, including the establishment
135 of a network of 47 meteorological sensors [46]. The authors compared both LCZ and Urban

136 Climate Zone (UCZ) classifications [47,48] with a 150 m grid resolution. These results
137 showed that LCZ is the most applicable mapping method for the thermal clustering of urban
138 areas.

139 The LCZ classification is based on the average values of morphological urban parameters, as
140 defined by Oke [18]. We extracted most of the morphological urban and building data
141 required for LCZ identification from the detailed BD TOPO database in France (database
142 from IGN, <http://professionnels.ign.fr/bdtopo>), and from OpenStreetmap [49]. Collecting
143 precise data on green areas and identifying trees was more challenging. To tackle this
144 problem, Haala and Brenner [50] proposed an imagery data methodology for urban areas. We
145 defined the main building typologies from local surveys and the TABULA project database
146 (<http://webtool.building-typology.eu/>). The definition of thermal properties at this urban zone
147 scale requires simplifications, especially given the strong variation in surface properties, such
148 as the albedo. For anthropogenic heat release in the district, we used the typical value from
149 the literature of about 8 W/m², which was measured in Toulouse, a city located in southwest
150 France [51,52].

151 According to the classification available online (mapuce.orbisgis.org), La Rochelle is
152 characterized by low and mid-rise buildings. Most of the downtown buildings are low-rise
153 residential constructions (height 3 to 6 m), while some suburban constructions are higher. We
154 studied an urban area located around the university (Figure 3a,b), close to the city center.



155

156

Figure 3: Aerial view (a), and digital model (b) for the neighborhood studied in La Rochelle.

157

We delimited the area of the case-study neighborhood within a 200 m radius (Figure 3a) to

158

extract morphological data from the BDTPOPO database (GIS). No available database was

159

available to determine green areas accurately and to provide all the necessary parameters. We

160

therefore built a digital model enhanced with simple vegetation modelling (Figure 3b).

161

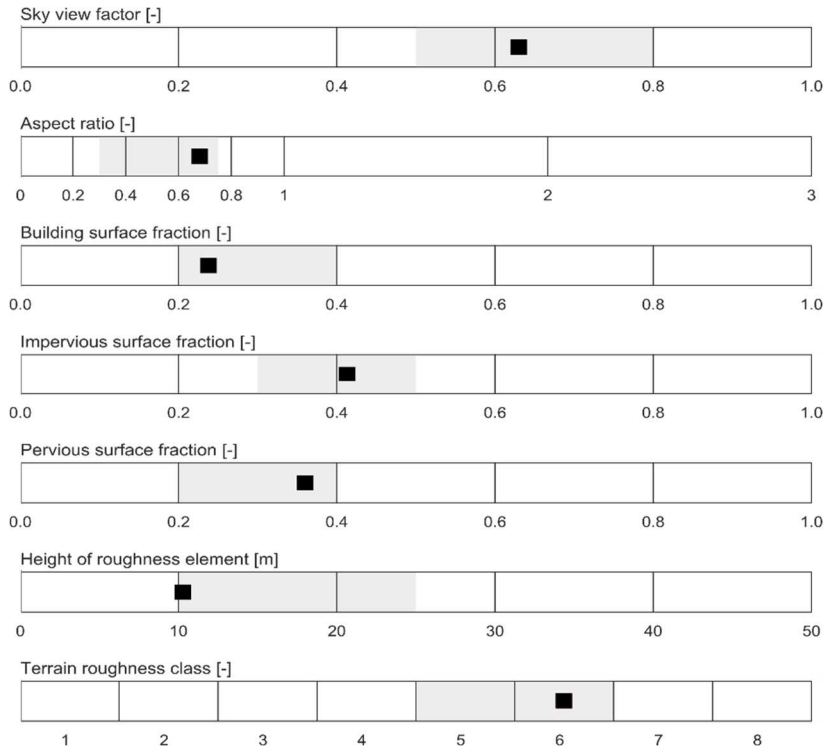
Finally, the case-study of the university neighborhood (Figure 3a,b) was determined as LCZ

162

type 5. The main parameters computed for this case-study and their variation range for LCZ 5

163

are presented in Figure 4.



164

165

Figure 4: Range values for LCZ 5 and parameters calculated according to Oke [18]

166

We computed for this urban area a plan-area density of 27 %, defined as the ratio of building

167

plan area to total plan area (%) [53], and an average building height of 11.6 m. This first step

168

characterizes an LCZ and the associated neighborhood UHI risk. Due to the lack of available

169

data and tools to quantify several urban parameters, this estimation may have significant

170

uncertainties. For example, green areas vary throughout the year, which was not taken into

171

account in the model, and this may impact the pervious surface fraction. Leconte [54] recently

172

highlighted similar limitations.

173 2.3 Measurement and urban model

174 2.3.1 Weather station technology

175

We collected weather data from the urban and rural weather stations (Figure 1) over the

176

summer period from June 1 to September 1, 2019. The rural station, located in a residential

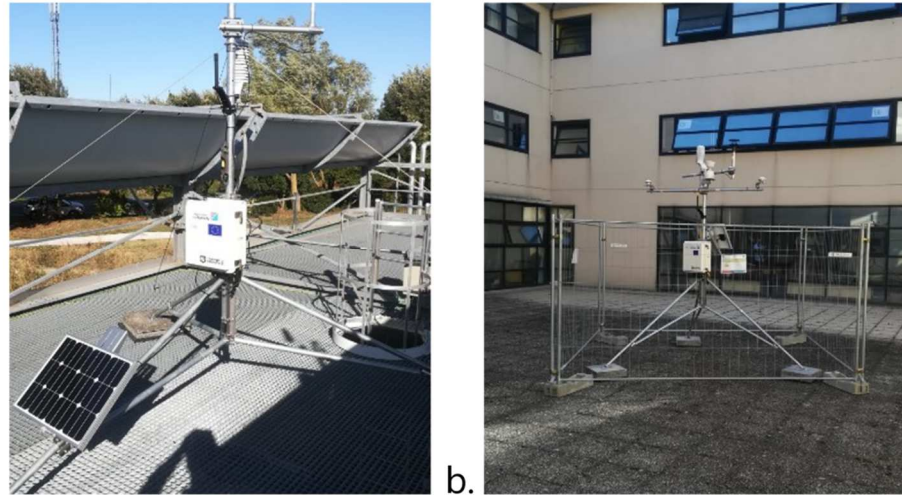
177

area in the northeast of La Rochelle, served as a reference station and is approximately 10 km

178

away from urban areas. Both urban weather stations (ULR₁ and ULR₂) in La Rochelle are in

179 the LCZ type 5 defined in the previous section. These urban weather stations are close to the
 180 sea (500 m approximately). The ULR₁ station is in an open field surrounded by trees and
 181 grass, while the ULR₂ station is located in the courtyard of a building (Figure 5a); ULR₂ is
 182 therefore shadier than ULR₁ (Figure 5b).



183 a. 184 b. Figure 5: ULR₁ (a) and ULR₂ (b) weather stations

185 The weather stations are composed of Campbell Scientific dataloggers and sensors (Table 1).
 186 The air temperature and humidity sensors were positioned at a height of 2 m.

187 Table 1 : Weather parameters and sensors for weather stations

Parameter	Sensor	Uncertainty
Air temperature [°C]	Rototronic© thermocouple HC2A-S3	0.1 °C
Relative humidity [%]	Rototronic© humidity sensors HC2A-S3	1%
Solar irradiance [W/m ²]	Kipp and Zonen© pyranometer CMP 3	2.6 %
Longwave irradiance [W/m ²]	Kipp and Zonen© pyrgeometer CMP 3	6.2 %
Wind direction	Windsonic© ultrasonic wind sensor WINDSONIC-LC Gill 2-D	-
Wind speed	Met One Instruments© wind anemometer 014A	-
Rainfall	Campbell© Kalyx-RG	-

188
 189 The suppliers provided the uncertainty of the solar shortwave and longwave sensors (Table 1).
 190 We performed a specific calibration for the relative humidity and the air temperature sensors.
 191 For the temperature, all the sensors were calibrated using a Fluke 7321 calibration bath that
 192 guarantees a 0.1 °C uncertainty between sensors. Similarly, humidity sensors were calibrated
 193 using LiCl and NaCl salts. Concerning other values, simultaneous recordings from all weather

194 stations demonstrated that the instruments provided the same output values for the same input
195 conditions.

196 2.3.2 Urban model

197 In order to complement the experimental analysis and further evaluate different passive
198 cooling strategies, the UWG model was used [19]. This model predicts the effects of the local
199 UHI for a specific urban zone. The physical UWG model is divided into four sub-models: (i)
200 a rural station model for heat flux calculation at a rural site; (ii) a vertical diffusion model for
201 vertical air profiles at the rural site; (iii) an urban boundary layer model for the calculation of
202 air temperature above the urban canyon; and (iv) a representative street canyon model to
203 compute the urban canopy and building energy sensible heat fluxes. Each sub-model is
204 represented by one node, and the street canyon model evaluates the average temperature
205 modification in an urban neighborhood. The model output is an urban weather file with
206 modified values of urban air temperature and relative humidity from a rural weather file.

207 The required input weather data, from the measurements at the rural weather station, include
208 ambient dry bulb temperature [$^{\circ}\text{C}$], relative humidity [%], wind direction [$^{\circ}$] and speed [m/s],
209 and rainfall [mm]. The horizontal direct and diffuse solar irradiances [W/m^2] were calculated
210 using the horizontal global solar irradiance measurements and the python pvlib library [55].
211 Finally, the direct normal irradiance and the solar position were estimated with the DISC
212 algorithm [56] and the PyEphem package [57].

213 The UWG model calculates the local UHI and overheating from a rural weather file. The
214 model was validated in the cities of Toulouse (France), Basel (Switzerland) [58], Rome and
215 Antofagasta (Italy) [20]. Furthermore, a study of the 2003 urban heatwave in downtown Paris
216 (France) gave a good correlation between UWG simulations and the measured temperatures
217 [7].

218 2.4 Urban planning strategies

219 2.4.1 Quantitative indicators

220 While no clear standard is available for urban planners, a large variety of tools and guidelines
221 are available to policy makers, such as in the US [59] and France [60], especially to answer
222 community requests relative to urban overheating issues. However, the spatial and temporal
223 results obtained from numerical simulations and measurements are too precise, and therefore
224 inappropriate to efficiently support stakeholders' decision-making. Martilli *et al.* [61] pointed
225 out the importance of looking at thermal stress in preference to UHI intensity as way to
226 propose heat mitigation strategies for urban stakeholders. While UHI intensity is useful
227 complementary information that quantifies the anthropogenic contribution to local climate
228 modification, the change in urban overheating in inhabited areas, especially during heatwaves,
229 is also a crucial indicator. We therefore propose to convert the detailed scientific data into two
230 easy-to-use indicators, initially to help fill the gap between the detailed evaluation and the
231 decision process:

- 232 • UHI exposure at the neighborhood scale, related to local microclimate warming;
- 233 • Neighborhood overheating related to heat thermal discomfort.

234 UHI has been quantified using different indicators in many research articles. Schwarz *et al.*
235 [62] discussed the relevance of eleven different surface UHI indicators, and noted a weak
236 correlations among them. UHI intensity is typically quantified by air or surface temperature
237 difference at a specific time-step between urban and reference rural weather stations [63–65]
238 (Eq. (1)). We decided to take into account UHI intensity rather than UHI exposure (UHI_{exp}
239 [$^{\circ}\text{C}\cdot\text{h}$], (Eq. (2)), which is a sum of positive differences between urban ($T_{\text{urb},t}$) and rural ($T_{\text{rur},t}$)
240 air temperatures.

$$\text{uhi}(t) = (T_{\text{urb},t} - T_{\text{rur},t})_{T_{\text{urb},t} > T_{\text{rur},t}} \quad (1)$$

$$\text{UHI}_{\text{exp}} = \sum_{t=0}^{n\Delta t} \text{uhi}(t) \times \Delta t \quad (2)$$

241 This cumulative intensity of UHI highlights the warming effect without the overstatements
 242 induced by maximum intensities at some specific periods.

243 The rural reference definition impacts UHI intensity [66], and was studied by Vogel and
 244 Afshari in the context of a coastal city [67]. They suggested different approaches:

- 245 ▪ The first approach is to locate both the reference rural and the urban weather stations
 246 at the same distance from the coast, as during sea-breeze events the coastal effect is
 247 also examined;
- 248 ▪ In the second approach, the reference is a virtual rural station located in an urban area
 249 without the city effects, which can be obtained only from simulations;
- 250 ▪ The third approach analyses an upstream rural reference station (related to wind
 251 direction), which gives similar results to the virtual reference method at nighttime.

252 In our approach, we used an inland reference rural weather station. Due to its location (see
 253 Figure 1), this reference is upstream during land breeze events. In contrast, during sea breeze
 254 events, the upstream reference station would be located in the sea, which is not relevant for
 255 our study since our aim was to characterize inhabited areas. Given that the purpose of this
 256 study was to determine the risk of an urban heat island for the inhabitants, we defined a rural
 257 station that could serve as a reference when the wind was inland (wind from the east). In this
 258 case, the city does not benefit from the refreshing marine breeze. Therefore, the positioning of
 259 the rural station makes it possible to evaluate the most unfavorable case concerning the risk of
 260 heat thermal discomfort.

261 For exposure to overheating, we adapted the Cooling Degree Hours indicator. This indicator,
 262 originally defined for the building energy sector, is also used to characterize local urban

263 climate [68]. Outdoor overheating affects both indoor and outdoor thermal comfort. We did
 264 not use thermal discomfort indexes (e.g., PMV, PET, or UTCI) due to the variety of locations
 265 and activities, and the vulnerability of urban inhabitants. As residents are usually indoors at
 266 night, the calculation of outdoor thermal discomfort is not relevant here. However, urban
 267 overheating during nighttime may be critical and lead to significant heat-related health
 268 impacts on the population.

269 The proposed overheating intensity was defined as the temperature difference between the air
 270 temperature ($T_{urb,t}$) and a threshold temperature ($T_{overheat}$). This temperature threshold was set
 271 at 26 °C during daytime, which is the cooling set-point for conditioned buildings as defined
 272 by the French thermal regulation [69]. Since nighttime-overheating exposure is more sensitive
 273 to the urban heat island, we also adopted a nighttime threshold of 21°C, a reference defined
 274 by the Heat Health Warning System heatwave for the city of La Rochelle. At each time step,
 275 the overheating intensity $oh(t)$ was quantified by the positive temperature difference between
 276 the outdoor air temperature and the threshold temperature, Eq. (3). Overheating exposure
 277 OH_{exp} , Eq. (4) is defined as the sum of the overheating intensities.

$$oh(t) = (T_{urb,t} - T_{overheat})_{T_{urb,t} > T_{overheat}} \quad (3)$$

$$OH_{exp} = \sum_{t=0}^{n\Delta t} oh(t) \times \Delta t \quad (4)$$

278

279 2.4.2 Sensitivity analysis

280 In construction or renovation projects, the neighborhood adaptation strategies and design must
 281 be analyzed through a multi-criteria analysis, which often lacks quantitative criteria and
 282 objective levers of action. In order to further guide adaptation strategies, sensitivity analysis
 283 (SA) helps to improve the understanding of model interactions and to identify the most
 284 relevant urban parameters in order to mitigate outdoor overheating and local UHI. The Morris
 285 method [70] has been used frequently in building design [71–73]. This method, also called the

286 elementary effects method, is a screening method used to estimate the elementary effects of
287 the input parameters roughly corresponding to a first-order partial derivative. For each
288 parameter studied, the Morris method evaluates the absolute average of the effects (μ^*)
289 corresponding to the mean effect of the parameter, as well as the standard deviation of these
290 effects (σ), which represents its interactions with the others parameters of interest (the
291 sampling method is based on an iterative variation of the parameters). All parameters are then
292 represented in the (σ - μ^*) plan for the analysis of the results. We used a grid-jump of 6 (level
293 of partition of the inputs domain) which was qualitatively estimated as sufficient to explore
294 the domain of the parameter space.

295 The first step was to define the possible design parameters for the neighborhood studied and
296 their bounds. In the literature, the morphological parameters have often been identified as
297 prominent for UHI; however, in a refurbishment context, these parameters cannot be modified
298 significantly. Other mitigation strategies have proven to be successful, such as an increase in
299 cool and green surfaces, and a reduction of anthropogenic heat. We assessed the influence of
300 five parameters, given fixed bounds: (i) road albedo (0.05 to 0.65); (ii) wall albedo (0.05 to
301 0.85); (iii) anthropogenic heat (2 to 20 W/m²); (iv) building height (7 to 13 m); and (v)
302 vegetation cover (0 to 85 %). We varied the building height to determine if adding one or two
303 floors to a building would impact the UHI intensity or overheating. Anthropogenic heat was
304 modulated following the default UWG weekly and daily schedule for urban traffic.

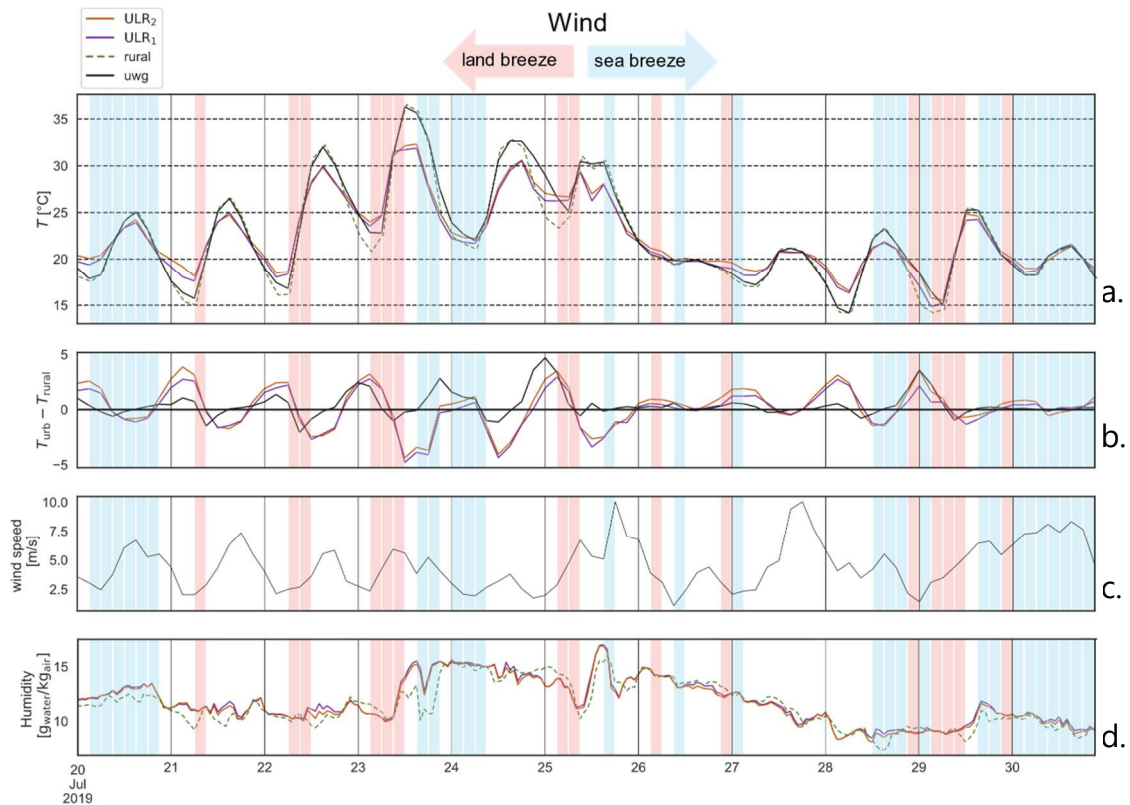
305 For the Morris method used here [70], we used a 100-trajectory sample , which corresponds to
306 500 simulations with the specified parameters and their discretization steps (we used a grid-
307 jump = 6). However, the SA approach is inconsistent for correlated parameters such as
308 vegetation cover and the average albedo of urban surfaces. To tackle this problem, we first
309 analyzed the albedo impact as a UHI mitigation strategy, given both the impact of the average

310 albedo for both roofs and walls. In the second step, we assessed the influence of vegetation
311 cover, without albedo modifications for non-vegetated surfaces.

312 **3 Results**

313 3.1 Local microclimate – urban and coastal effect

314 This section presents and analyses the measurements made during the heatwave, from the 20th
315 to the 30th July 2019. Figure 6 presents from top to bottom: air temperature, the temperature
316 difference between the urban and rural stations, wind speed, and specific humidity. We
317 compared the modelled temperatures (UWG) to the measurements, and we discuss the
318 reliability of the model for our case study. It seems that the direction of the wind coming
319 either from the sea or from the land affected the results, which is explained below. To
320 understand the influence of the wind, the sea breeze periods (NNW 337° to SSW 202°) are
321 highlighted in Figure 6 in blue, and the land breeze periods in red (NNE 22.5° to SSE 157.5°).



323

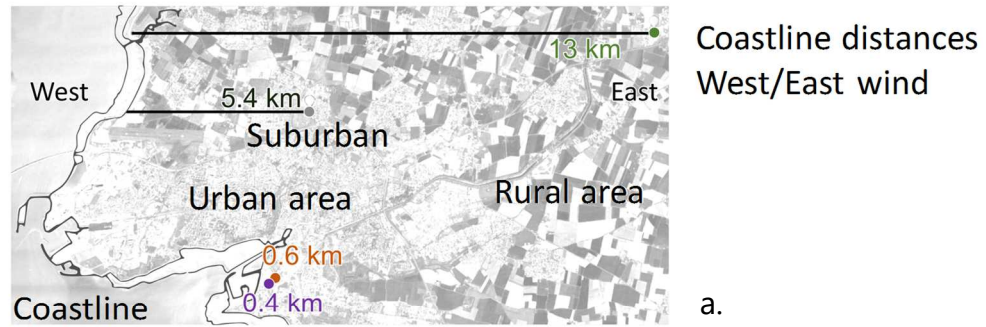
324 Figure 6: (a) Air temperature at the rural weather station for both urban weather stations during heatwave days in
 325 La Rochelle and predicted by the UWG model (b) Temperature differences between rural/urban areas both
 326 measured and predicted by the UWG model (c) Wind speed (d) Measured humidity

327 In Figure 6a, the urban heat island is recognizable during nighttime, where higher
 328 temperatures were recorded at both urban stations (ULR1 and ULR2) than at the rural station.
 329 A maximum of 4°C temperature difference was recorded during this period. The predicted
 330 urban night temperatures (UWG) were higher than the rural measurements but lower in
 331 comparison to the urban measurements. During the day the phenomenon was reversed, and
 332 the measured temperatures in the urban area were lower than in the countryside, as illustrated
 333 on Figure 6b. From July 20th to July 25th, the temperature difference between urban and rural
 334 areas was positive during nighttime and negative during daytime, up to almost 5°C cooler on
 335 the warmest days, July 23 and 24. The daily amplitude between temperature minima and
 336 maxima in the local neighborhood was, therefore, greatly reduced compared to the
 337 countryside.

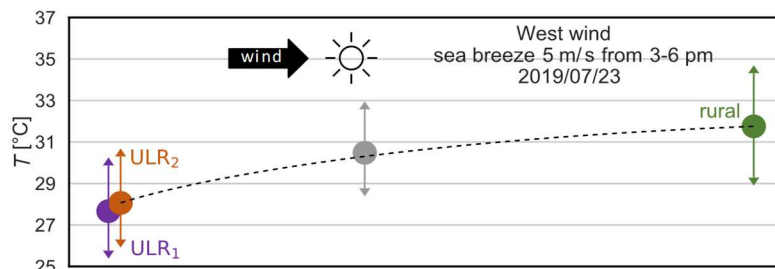
338 Daytime temperatures obtained from the UWG model were consistent with the rural weather
339 station records. The model confirmed this trend during the night, but overestimated the
340 temperature during daytime, especially on July 22nd, 23rd and 24th. To explore this divergence,
341 we analyzed the wind direction and intensity (Figure 6c). The sea breeze was more likely to
342 occur at the end of the day. With evaporation effects, this sea breeze contributed to a decrease
343 in the temperature of the urban area. These local mass flows due to the sea were not modelled
344 by the UWG model, which contributed to the observed divergences during daytime. Other
345 studies using the UWG model observed an overestimation of the heat island during the day
346 [74]. This overestimation may come from a poor assessment of the urban limit layer height,
347 which is a challenging parameter to estimate. An improvement in the vertical model has been
348 proposed recently [75].

349 This divergence was further investigated by analyzing the difference in absolute humidity
350 between urban and rural areas, as represented in Figure 6d. During sea breeze events, the
351 absolute humidity increased in the urban area, which contributed to the decrease in
352 temperatures (Figure 6d, see evenings on July 20th, 23rd, 25th, 28th and 29th). The phenomenon
353 rarely occurred during land breeze events.

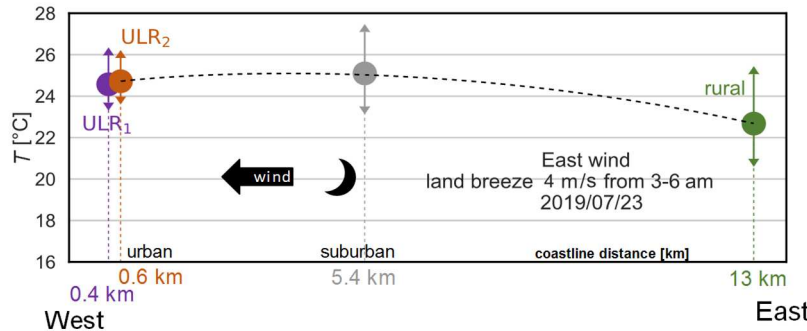
354 The influence of wind direction is more specifically addressed in Figure 7, during the hottest
355 day of the heatwave under study (July 23rd).



a.



b.



c.

356

357 Figure 7: Day and night temperature distribution for 4 urban, suburban and rural weather stations, during the
358 hottest day of the heatwave (July 23rd, 2019)

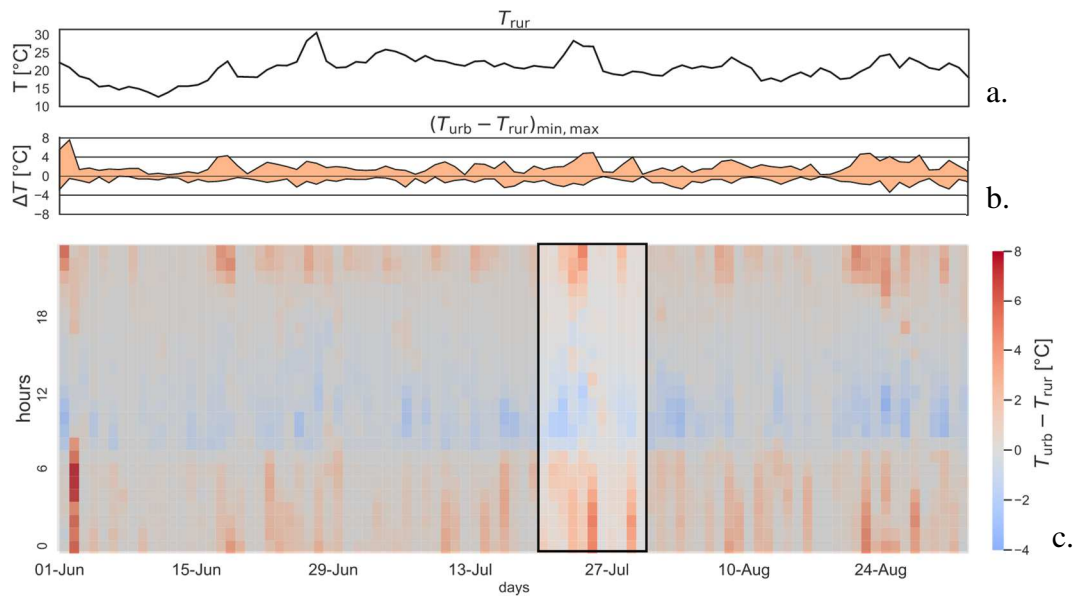
359 The coastline distance (Figure 7a) was defined for each weather station as the distance from
360 the sea along the wind direction (from east and from west). The temperature values for
361 specific periods of the day are represented for urban, suburban and rural areas, given the
362 coastline distance (Figure 7b-c). At 5.4 km from the coastline (grey point), an additional
363 suburban weather station was available in an industrial area north of La Rochelle (Figure 7a),
364 identified as an LCZ 8. In Figure 7b, the temperatures were averaged over the three-hour
365 interval in the afternoon, 3 PM to 6 PM, identified as a sea breeze event from the wind
366 direction records. The arrows represent the minimum and maximum temperature intervals for
367 this period. For the three-hour night period, from 3AM to 6 AM (Figure 7c), we observed a

368 land breeze event. During this night period, the air temperature decreased with the coastline
369 distance from the urban, to the suburban, and to the rural stations. An average difference of
370 2°C was observed between the urban and rural areas during the night. The suburban air
371 temperature increased slightly due to the stronger local UHI effect and the reduced sea
372 cooling effect, reinforced by the absence of a sea breeze and the greater distance from the
373 coast compared to the urban location.

374 3.2 Urban heat island and overheating intensity

375 In this section, we analyze the experimental and numerical results using the previously
376 defined indicators.

377 First, for the UHI intensity (see 2.4.1), the hourly rural temperature variation and the
378 temperature difference $\Delta T = T_{\text{urb}} - T_{\text{rur}}$, estimated with the UWG model, are represented in
379 Figure 8 for the summer (from June 1st to September 1st, 2019). Figure 8-a represents the rural
380 temperature, Figure 8-b represents the daily maximum and minimum temperature differences,
381 and Figure 8-c represents the hourly temperature difference distribution. The previously
382 studied heatwave period is highlighted in black in Figure 8-c.

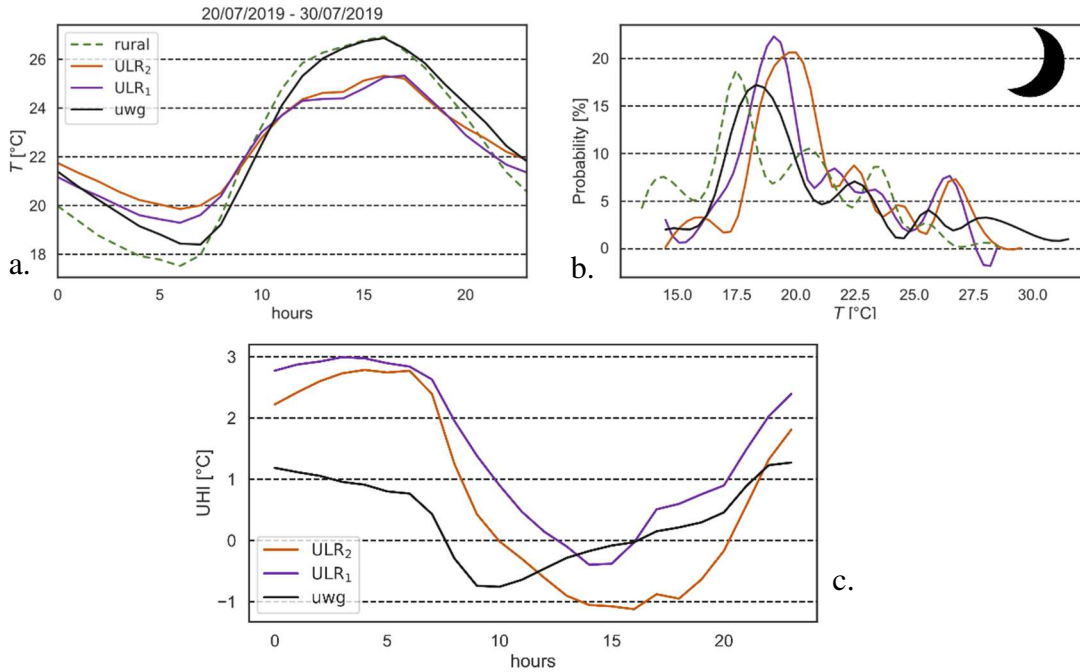


384

385 Figure 8: Daily rural temperature (a), daily maximum/minimum UHI temperature difference (b), and hourly UHI
 386 temperature difference (c) for the La Rochelle University location, obtained with the UWG model, from June 01
 387 to September 01.

388 In Figure 8-c, the cool island effects ($\Delta T < 0$) were observed between 7 AM and 6 PM (blue
 389 color, these values were excluded from the UHI_{exp} calculation). The urban local microclimate
 390 is often cooler than the rural area during daytime, which is due to the thermal mass of the
 391 buildings and the shadow effects in the urban context that are taken into account by the UWG
 392 model. However, the daytime hourly cooling effect from the UWG model was underestimated
 393 compared to the measurements, as UWG does not account for the presence of the sea. The
 394 UHI (red-colored hours) mainly occurred at night. In comparison with the measurements, for
 395 both urban locations (ULR_1 and ULR_2), UHI exposure (UHI_{exp}) during the heatwave (July
 396 20th to 30th, 2019) was around seven times higher during nighttime than daytime. During this
 397 period, the modelled values (Figure 8-c) of the nighttime UHI_{exp} (128 °C.h) were slightly
 398 underestimated compared to the experimental UHI_{exp} values, 153 °C.h and 213 °C.h for ULR_1
 399 and ULR_2 , respectively.

400 For the same period, Figure 9a presents the average daily temperature profile obtained from
 401 ULR₁, ULR₂, and the rural weather stations, and the modelled urban area with UWG. Figure
 402 9b presents the temperature distribution during the same heatwave for the UHI at night.

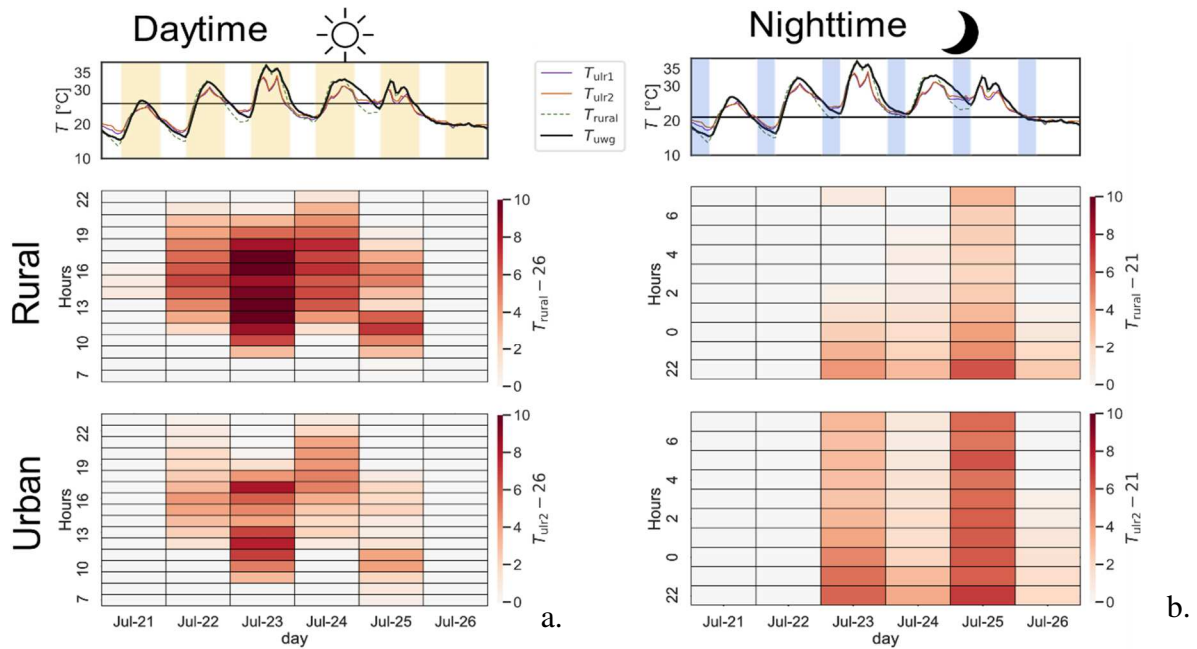


403
 404 Figure 9: (a) Daily temperature profile for ULR₁, ULR₂, the rural weather station and UWG (from July 20 to 30,
 405 2019), (b) The probability distribution for nighttime temperature and (c) The UHI distribution for ULR₁, ULR₂
 406 and UWG

407 At night, the UHI effect observed by the model was close to the measurements, and the
 408 temperature in urban areas was 1.5 °C higher than in rural areas. (Figure 9a). The variation in
 409 UWG temperature was consistent with the measurement from 10 PM to 4 AM. However, as
 410 previously observed (Figure 6), the early morning temperatures were underestimated by the
 411 model, while the calculated temperatures did not represent correctly the observed daytime
 412 temperature decrease in an urban context, which was due to the coastal effects.

413 In terms of outdoor overheating (defined in 2.4.1), and focusing on the hottest days (from July
 414 21st to July 26th, 2019), Figure 10 shows the hourly variation of the OH_{exp} for both the rural
 415 and urban weather station ULR₂. The figure shows the temporal series of ULR₁, ULR₂, the
 416 rural stations and UWG. In addition, we chose to present heatmaps of the indicators,

417 comparing the rural and the ULR₂ weather stations; ULR₂ was selected because it is in a more
 418 urbanized location than URL₁ and has a higher risk of overheating.



419
 420 Figure 10: Hourly temperature variation (top), and hourly overheating variation for rural and urban (bottom) -
 421 during daytime (a) and nighttime (b) - from July 21st to July 26th

422 The hourly temperature variation is presented at the top of Figure 10. The periods are
 423 highlighted in yellow for daytime (7 AM to 10 PM, Figure 10a) and in blue for nighttime
 424 (10 PM to 6 AM, Figure 10b). During daytime (Figure 10a), the rural area was more
 425 vulnerable to the heatwave than the urban area (ULR₂). On July 23rd (daytime), the maximum
 426 overheating intensity reached +10 °C at the rural station, while that of urban stations close to
 427 the coast and cooler than the rural stations was only + 7 ° C. In contrast, nighttime
 428 overheating was higher in the urban area, where it increased up to +6.3 °C, compared to +4
 429 °C at the rural station. This maximum nighttime overheating (Figure 10b) was observed two
 430 days later (July 25th). For the hottest day (July 23rd), urban nighttime overheating remained
 431 much lower than rural overheating. Over the period, urban (ULR₂) daytime overheating
 432 ($OH_{exp} = 140 \text{ } ^\circ\text{Ch}$) was 45 % lower than that in the rural area ($OH_{exp} = 249 \text{ } ^\circ\text{Ch}$). Nighttime

433 overheating for the urban area was well quantified by the same OH_{exp} indicator, which was
 434 95 % higher than the rural indicator, 126 °Ch and 64 °Ch, respectively.

435 Table 2 summarizes the UHI_{exp} and OH_{exp} indicators for daytime and nighttime as well as for
 436 different urban/rural areas and the UWG model.

437 Table 2: UHI_{exp} and OH_{exp} indicators for daytime and nighttime, obtained from the urban weather stations
 438 (ULR_1 and ULR_2) and the model (UWG), for the heatwave period (July 20th to 30th, 2019)

		ULR₁	ULR₂	UWG	rural
UHI_{exp} [°C.h]	Day	20	25	29	-
	Night	153	213	128	-
OH_{exp} [°C.h]	Day	133	140	248	249
	Night	107	126	134	64

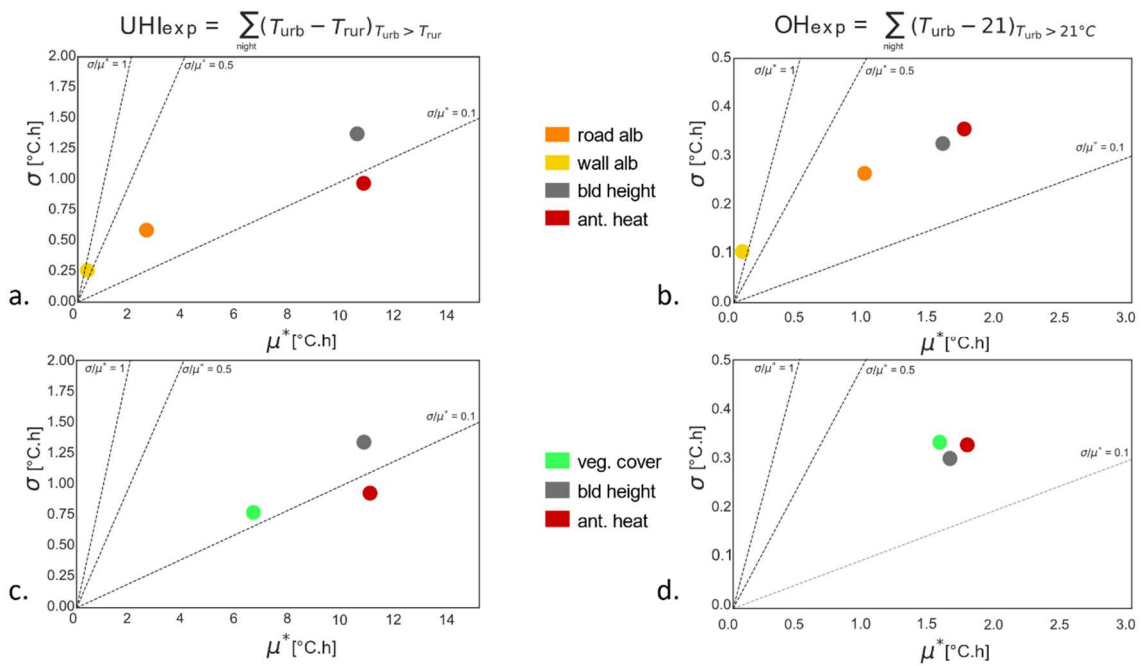
439
 440 Within the same LCZ 5 neighborhood (ULR_1 and ULR_2 weather stations), the UHI_{exp} was
 441 amplified from day to night by a factor of about seven. However, significant UHI_{exp}
 442 differences were observed between ULR_1 and ULR_2 , with 25 % for daytime and 39 % for
 443 nighttime, respectively (Table 2). This can be explained by the vegetated area surrounding the
 444 ULR_1 weather station, which was also more exposed to winds, while the ULR_2 weather
 445 station was located within a courtyard surrounded by buildings. While the simplified UWG
 446 model was not consistent with daily urban temperature variations (grayed in Table 2), this
 447 approach gave a good representation of the nighttime variations.

448 Overheating exposure was much more homogeneous within the neighborhood under study, as
 449 observed for ULR_1 and ULR_2 , with a 5 % OH_{exp} difference for daytime, and a 18 % OH_{exp}
 450 difference for nighttime (Table 2). As expected, the simplified modelling approach (UWG)
 451 significantly overestimated daytime overheating. However, this model (UWG) gave a good
 452 assessment of nighttime overheating compared to the urbanized area, represented by the ULR_2
 453 station, where the overestimation of the nighttime OH_{exp} was only about 6%.

454 Therefore, the modelling approach and the proposed indicators were further analyzed during
 455 nighttime for the UHI intensity and overheating effects.

456 3.3 Neighborhood design parameters

457 The key urban parameters for this case study, for both the intensity of outdoor overheating
 458 and UHI (OH_{exp} and UHI_{exp}), were identified using the sensitivity analysis (SA) results
 459 (Figure 11). The SA objective functions (OH_{exp} and UHI_{exp}) were numerically determined
 460 with the UWG model, over the nighttime summer period from June 1st to September 1st.
 461 Indeed, we excluded the daytime periods as they include sea breeze events not taken into
 462 account by the model. This was observed in the experimental comparison of OH_{exp} and
 463 UHI_{exp} (Table 2). The SA model inputs are the urban design parameters, and its output
 464 objective function is either the indicator UHI_{exp} , or OH_{exp} . The UWG model was run several
 465 times through the Morris design matrix to identify the most influential parameters. The SA
 466 results provided the average variation μ^* [$^{\circ}Ch$] (x-axis) and the standard deviation σ [$^{\circ}Ch$] (y-
 467 axis) of the elementary effects for each parameter. A parameter effect is considered as almost
 468 linear if $\sigma / \mu^* < 0.1$, quasi-monotonic if $0.5 < \sigma / \mu^* < 1$, and non-monotonic (i.e., interactions
 469 with other parameters) if $\sigma / \mu^* > 1$. If $\sigma / \mu^* < 0.5$, the parameter can be considered as
 470 independent from the other parameters.



471

472 Figure 11: sensitivity analysis for UHI intensity (left) and overheating (right) - for albedo strategies (top) and
473 vegetation (bottom) - from July 20th to 30th, 2019.

474 The results for UHI exposure for the nighttime summer period (Figure 11a,c) for variations in
475 both albedo and vegetation cover, suggest that the parameters are independent, with an almost
476 linear effect. The height of the buildings, anthropogenic heat and vegetation cover were the
477 parameters that had the most impact, regarding the absolute values μ^* . This means that, of the
478 parameters studied, these have the highest potential to mitigate urban heat stress. The road
479 and wall albedo had a smaller effect, which could be due to the lower impacts of daily solar
480 heat gain over the nighttime period for this case study. For the overheating exposure OH_{exp}
481 during the nighttime summer period (Figure 11b,d), the key parameter sensitivities were
482 similarly classified, except road albedo (orange point, Figure 11) and vegetation cover (green
483 point, Figure 11), which had a relative increased sensitivity. While the impacts of vegetation
484 on the urban microclimate are well documented, this approach highlights possible differences
485 depending on the indicator of interest. The importance of urban morphology parameters was
486 also emphasized by Salvati *et al.*[20] using the UWG model. While the use of the Morris
487 method requires a certain expertise, the results can easily be used by city stakeholders to rank
488 the impact of the parameters on urban overheating. These help to identify the main strategies
489 that should be implemented to mitigate the hot spots of a city previously identified during the
490 mapping of the urban zones (Figure 2). Therefore, this method helps establish priorities in the
491 plans of action.

492 **4 Discussion**

493 For this coastal city case study, the measurements revealed a cooling sea breeze effect during
494 the daytime. Although both ULR₁ and ULR₂ weather stations were close to each other and
495 had similar variations in temperature, significant differences were obtained for both UHI and
496 overheating exposure. These results highlight the impact of the thermal heterogeneity of the
497 urban environment. Moreover, beyond the usual characterization of a LCZ, the indicators

498 obtained show that the evaluation of the risk of overheating in inhabited places may require
499 multiplying the measurement points within this LCZ.

500 Similarly to our case study, the littoral urban microclimate was characterized in Sydney by
501 Khan *et al.* [76] during a heatwave in 2017. A significant difference of 10 °C was measured
502 between urban and rural areas. Wind intensity and direction were identified as key parameters
503 for the advective heat fluxes. It was observed that the humidity difference between the urban
504 zone and the rural surroundings was also an important factor affecting the urban
505 microclimate. Unlike our case study, Khan *et al.* observed a higher UHI intensity during
506 daytime, which they explained by the surrounding desert of Sydney. Yet, the same cooling-
507 down effect was observed at the end of the night at the coastal stations. Founda and
508 Santamouris [8] observed sea breeze effects on the urban air temperature and humidity for the
509 Mediterranean city of Athens, Greece. They underlined the fact that the water heat capacity
510 dampens the daily temperature variations and the daytime UHI, as in Figure 9a. This
511 phenomenon was also noted by Long *et al.* [7] during the ESCOMPTE project for the
512 Mediterranean city of Marseille, France. While our measurements confirm the tendencies
513 found in other studies, the main findings of this case study concern the variations in exposure
514 (Table 2), especially between day and night. The comparison of this evaluation process for
515 other locations and cities will give a better understanding of the variation in amplitude of
516 these exposure indicators.

517 From a modelling point of view, UWG is a practical tool for comparing urban design options,
518 based on a reduced number of inputs. However, as a counterpart to the simplicity of this one-
519 node model at the neighborhood scale, it cannot englobe the spatial heterogeneity for a deeper
520 analysis within the zone, nor account for the regional surroundings, such as large bodies of
521 water. Indeed, a comparison of the two urban stations revealed episodic differences. More
522 complex models could be used [77], with a refined spatial resolution to access urban fabric

523 temperature distribution, more realistic shadow effects, and wind patterns. Yet, such a
524 detailed analysis is not suitable for decision support for stakeholders in the initial steps of the
525 design stage. So, determining the tendencies of the impacts of these simple design parameters,
526 such as vegetation cover, will then guide urban planners for much more detailed plans, given
527 the complex urban constraints that cannot be taken into account in the extensive sensitivity
528 analysis. In a further step, new or innovative greening techniques could, for example, be used
529 to maximize the vegetation effects identified here.

530 The adaptation strategies suggested by the SA results are highly dependent on the period of
531 investigation, the indicators, and the range of variation of the input parameters. The proposed
532 SA was restricted to the nighttime periods, which was relevant for this case-study as the UHI
533 intensity was higher at night. The results showed that vegetation cover, the height of the
534 buildings, and anthropogenic heat had the most impact on the variations in UHI_{exp} and OH_{exp} .
535 The results may differ for other cities with higher daytime UHI effects or other indicators,
536 such as the surface UHI effect.

537 **5 Conclusions**

538 We propose a methodology that meets the need to characterize the UHI effect at the
539 neighborhood scale. This methodology was used in a coastal case-study of the university
540 neighborhood in La Rochelle, close to the city center. An extended study including additional
541 weather stations within the city is ongoing. While the coastal effect demonstrated a mitigation
542 effect during the daytime, the UHI was more pronounced during nighttime, which is expected
543 in French cities. The measurements revealed a nocturnal UHI effect, with an average
544 temperature increase of +2 °C, which reached +8 °C on the warmest days. This high increase
545 during a heatwave stresses the importance of this work, which is designed to provide key
546 indicators and general guidelines for stakeholders to reduce urban heat stress during future
547 heatwaves. Both UHI and overheating intensities were studied and quantified through UHI_{exp}

548 and OH_{exp} indicators, which we defined to assist the analysis of the results. The UHI intensity
549 increased by seven from day to night for both urban locations. The urban outdoor overheating
550 exposure, quantified by the sum of urban hourly air temperatures above specific daytime and
551 nighttime thresholds, was higher during daytime. The experimental part of this research work
552 highlighted the pitfalls to avoid in order to improve measurement reliability. The
553 methodology could be enriched with a more detailed urban microclimate model.

554 The analysis highlighted non-negligible differences in these indicators between the two urban
555 weather stations, located within the same LCZ. These results are limited to a single case
556 study, yet they are consistent with more extensive studies on temperature variation within
557 LCZs [45]. While the LCZ scale is a useful initial approach to roughly classify a city into
558 zones with UHI or overheating risks, as proposed in our methodology (see Figure 2), and to
559 analyze the various neighborhood scale strategies (see section 3.3), urban planners need to
560 assess more precisely the risk of overheating at the building or inhabitant scale. The
561 experiments confirmed the ability of both aggregated and simple indicators to capture local
562 variations. They have the potential to be a convenient tool for the evaluation of urban
563 strategies. Furthermore, this emphasizes the need to be cautious when using LCZ-scale results
564 in implementing urban cooling strategies.

565 The consistency of the UWG model in representing nighttime UHI and overheating
566 intensities, in comparison with the measurements made it possible to study the sensitivity of
567 several urban design parameters during the extended summer period. The results showed that
568 anthropogenic heat release, vegetation cover and the height of buildings were key design
569 parameters that need to be taken into account in order to mitigate the local microclimate air
570 temperature in a given neighborhood. The adaptation strategies we identified could help to
571 define strategies to mitigate the expected increase of UHI and outdoor overheating, while the

572 precise detection of hot spots will provide insights into where it is most efficient to implement
573 these strategies.

574 **6 Acknowledgements**

575 This study was partially funded by the EQL'ORE project supported by the Region of
576 Nouvelle Aquitaine, and the European FEDER project PEDOBUR. We acknowledge M.
577 Burlot for his contribution and his great expertise in the sensor calibration and weather station
578 selection. We also acknowledge the UWG software developers and the developers of the
579 Python SALib library.

580 **7 References**

- 581 [1] K.C. Seto, M. Fragkias, B. Güneralp, M.K. Reilly, A Meta-Analysis of Global Urban Land
582 Expansion, PLOS ONE. 6 (2011) e23777. <https://doi.org/10.1371/journal.pone.0023777>.
- 583 [2] M. Santamouris, Energy and Climate in the Urban Built Environment, Routledge, 2013.
- 584 [3] H.H. KIM, Urban heat island, International Journal of Remote Sensing. 13 (1992) 2319–
585 2336. <https://doi.org/10.1080/01431169208904271>.
- 586 [4] C. Heaviside, S. Vardoulakis, X.-M. Cai, Attribution of mortality to the urban heat island
587 during heatwaves in the West Midlands, UK, Environmental Health. 15 (2016) S27.
588 <https://doi.org/10.1186/s12940-016-0100-9>.
- 589 [5] J. Paravantis, M. Santamouris, C. Cartalis, C. Efthymiou, N. Kontoulis, Mortality Associated
590 with High Ambient Temperatures, Heatwaves, and the Urban Heat Island in Athens,
591 Greece, Sustainability. 9 (2017) 606. <https://doi.org/10.3390/su9040606>.
- 592 [6] X.-M. Hu, M. Xue, Influence of Synoptic Sea-Breeze Fronts on the Urban Heat Island
593 Intensity in Dallas–Fort Worth, Texas, Mon. Wea. Rev. 144 (2015) 1487–1507.
594 <https://doi.org/10.1175/MWR-D-15-0201.1>.
- 595 [7] N. Long, G. Pigeon, P.G. MESTAYER, P. Durand, C. Kergomard, Correlation between
596 temperature and classification of urban fabric on Marseille during ESCOMPTE, in: 5th
597 International Conference on Urban Climate, Lodz, Poland, 2003. [https://hal.archives-
598 ouvertes.fr/hal-01155989](https://hal.archives-ouvertes.fr/hal-01155989) (accessed May 15, 2020).
- 599 [8] D. Founda, M. Santamouris, Synergies between Urban Heat Island and Heat Waves in
600 Athens (Greece), during an extremely hot summer (2012), Scientific Reports. 7 (2017)
601 10973. <https://doi.org/10.1038/s41598-017-11407-6>.
- 602 [9] G. Ulpiani, On the linkage between urban heat island and urban pollution island: Three-
603 decade literature review towards a conceptual framework, Science of The Total
604 Environment. 751 (2021) 141727. <https://doi.org/10.1016/j.scitotenv.2020.141727>.
- 605 [10] B.-J. He, J. Wang, H. Liu, G. Ulpiani, Localized synergies between heat waves and urban
606 heat islands: Implications on human thermal comfort and urban heat management,
607 Environmental Research. 193 (2021). <https://doi.org/10.1016/j.envres.2020.110584>.
- 608 [11] P. Kristensen, European Environment Agency, Climate change, impacts and vulnerability
609 in Europe 2012: an indicator-based report, Publications Office, Luxembourg, 2012.

- 610 [12] S. Kovats, T. Wolf, B. Menne, Heatwave of August 2003 in Europe: provisional estimates
611 of the impact on mortality, *Weekly Releases (1997–2007)*. 8 (2004) 2409.
612 <https://doi.org/10.2807/esw.08.11.02409-en>.
- 613 [13] J.-M. Robine, S.L.K. Cheung, S. Le Roy, H. Van Oyen, C. Griffiths, J.-P. Michel, F.R.
614 Herrmann, Death toll exceeded 70,000 in Europe during the summer of 2003, *C. R. Biol.*
615 331 (2008) 171–178. <https://doi.org/10.1016/j.crv.2007.12.001>.
- 616 [14] K. Laaidi, A. Zeghnoun, B. Dousset, P. Bretin, S. Vandentorren, E. Giraudet, P. Beaudeau,
617 The Impact of Heat Islands on Mortality in Paris during the August 2003 Heat Wave,
618 *Environ Health Perspect.* 120 (2012) 254–259. <https://doi.org/10/dpkxqr>.
- 619 [15] The SW Ecodistrict, *A Vision Plan for a More Sustainable Future*, (n.d.) 122.
- 620 [16] EcoDistricts | AustinTexas.gov, (n.d.).
621 <https://www.austintexas.gov/departments/ecodistricts-0> (accessed September 13, 2021).
- 622 [17] A. Machard, S. Martinez, E. Bozonnet, E. Lacedra, C. Inard, How to assess ecodistrict
623 resilience to urban heat stress under future heatwaves? A case study for the city of
624 Paris., 1st International Conference on Climate Resilient Built Environment-ICRBE, 21-23
625 September 2020, Bali, Indonesia. 1st International Conference on Climate Resilient Built
626 Environment-ICRBE, 21-23 September 2020, Bali, Indonesia (2020).
- 627 [18] I.D. Stewart, T.R. Oke, Local Climate Zones for Urban Temperature Studies, *Bulletin of*
628 *the American Meteorological Society.* 93 (2012) 1879–1900.
629 <https://doi.org/10.1175/BAMS-D-11-00019.1>.
- 630 [19] A. Nakano, B. Bueno, L. Norford, C.F. Reinhart, Urban Weather Generator - a Novel
631 Workflow for Integrating Urban Heat Island Effect within Urban Design Process, MIT
632 Web Domain. (2015). <https://dspace.mit.edu/handle/1721.1/108779> (accessed July 29,
633 2020).
- 634 [20] A. Salvati, M. Palme, G. Chiesa, M. Kolokotroni, Built form, urban climate and building
635 energy modelling: case-studies in Rome and Antofagasta, *Journal of Building*
636 *Performance Simulation.* 13 (2020) 209–225.
637 <https://doi.org/10.1080/19401493.2019.1707876>.
- 638 [21] M. Palme, L. Inostroza, G. Villacreses, A. Lobato-Cordero, C. Carrasco, From urban
639 climate to energy consumption. Enhancing building performance simulation by
640 including the urban heat island effect, *Energy and Buildings.* 145 (2017) 107–120.
641 <https://doi.org/10.1016/j.enbuild.2017.03.069>.
- 642 [22] J. Parker, The Leeds urban heat island and its implications for energy use and thermal
643 comfort, *Energy and Buildings.* 235 (2021) 110636.
644 <https://doi.org/10.1016/j.enbuild.2020.110636>.
- 645 [23] A. Boccalatte, M. Fossa, L. Gaillard, C. Menezo, Microclimate and urban morphology
646 effects on building energy demand in different European cities, *Energy and Buildings.*
647 224 (2020) 110129. <https://doi.org/10.1016/j.enbuild.2020.110129>.
- 648 [24] S. Tsoka, K. Tolika, T. Theodosiou, K. Tsikaloudaki, D. Bikas, A method to account for the
649 urban microclimate on the creation of ‘typical weather year’ datasets for building energy
650 simulation, using stochastically generated data, *Energy and Buildings.* 165 (2018) 270–
651 283. <https://doi.org/10.1016/j.enbuild.2018.01.016>.
- 652 [25] L.G.R. Santos, A. Afshari, L.K. Norford, J. Mao, Evaluating approaches for district-wide
653 energy model calibration considering the Urban Heat Island effect, *Applied Energy.* 215
654 (2018) 31–40. <https://doi.org/10.1016/j.apenergy.2018.01.089>.

- 655 [26] L.G.R. Santos, I. Nevat, G. Pignatta, L.K. Norford, Climate-informed decision-making for
656 urban design: Assessing the impact of urban morphology on urban heat island, *Urban*
657 *Climate*. 36 (2021) 100776. <https://doi.org/10.1016/j.uclim.2021.100776>.
- 658 [27] A. Salvati, M. Palme, G. Chiesa, M. Kolokotroni, Built form, urban climate and building
659 energy modelling: case-studies in Rome and Antofagasta, *Journal of Building*
660 *Performance Simulation*. 13 (2020) 209–225.
661 <https://doi.org/10.1080/19401493.2019.1707876>.
- 662 [28] L. Chapman, J.A. Azevedo, T. Prieto-Lopez, Urban heat & critical infrastructure networks:
663 A viewpoint, *Urban Climate*. 3 (2013) 7–12. <https://doi.org/10.1016/j.uclim.2013.04.001>.
- 664 [29] T.R. Oke, City size and the urban heat island, *Atmospheric Environment* (1967). 7 (1973)
665 769–779. [https://doi.org/10.1016/0004-6981\(73\)90140-6](https://doi.org/10.1016/0004-6981(73)90140-6).
- 666 [30] M. Santamouris, Recent progress on urban overheating and heat island research.
667 Integrated assessment of the energy, environmental, vulnerability and health impact.
668 Synergies with the global climate change, *Energy and Buildings*. 207 (2020) 109482.
669 <https://doi.org/10.1016/j.enbuild.2019.109482>.
- 670 [31] M. Santamouris, C. Cartalis, A. Synnefa, D. Kolokotsa, On the impact of urban heat island
671 and global warming on the power demand and electricity consumption of buildings—A
672 review, *Energy and Buildings*. 98 (2015) 119–124.
673 <https://doi.org/10.1016/j.enbuild.2014.09.052>.
- 674 [32] T. Susca, S.R. Gaffin, G.R. Dell’Osso, Positive effects of vegetation: Urban heat island and
675 green roofs, *Environmental Pollution*. 159 (2011) 2119–2126.
676 <https://doi.org/10.1016/j.envpol.2011.03.007>.
- 677 [33] S. Bonafoni, G. Baldinelli, P. Verducci, Sustainable strategies for smart cities: Analysis of
678 the town development effect on surface urban heat island through remote sensing
679 methodologies, *Sustainable Cities and Society*. 29 (2017) 211–218.
680 <https://doi.org/10.1016/j.scs.2016.11.005>.
- 681 [34] H. Taha, H. Akbari, A. Rosenfeld, J. Huang, Residential cooling loads and the urban heat
682 island—the effects of albedo, *Building and Environment*. 23 (1988) 271–283.
683 [https://doi.org/10.1016/0360-1323\(88\)90033-9](https://doi.org/10.1016/0360-1323(88)90033-9).
- 684 [35] A.G. Touchaei, M. Hosseini, H. Akbari, Energy savings potentials of commercial buildings
685 by urban heat island reduction strategies in Montreal (Canada), *Energy and Buildings*.
686 110 (2016) 41–48. <https://doi.org/10.1016/j.enbuild.2015.10.018>.
- 687 [36] E.J. Gago, J. Roldan, R. Pacheco-Torres, J. Ordóñez, The city and urban heat islands: A
688 review of strategies to mitigate adverse effects, *Renewable and Sustainable Energy*
689 *Reviews*. 25 (2013) 749–758. <https://doi.org/10.1016/j.rser.2013.05.057>.
- 690 [37] M. Santamouris, Using cool pavements as a mitigation strategy to fight urban heat
691 island—A review of the actual developments, *Renewable and Sustainable Energy*
692 *Reviews*. 26 (2013) 224–240. <https://doi.org/10.1016/j.rser.2013.05.047>.
- 693 [38] W.P. Lowry, Empirical Estimation of Urban Effects on Climate: A Problem Analysis,
694 *Journal of Applied Meteorology and Climatology*. 16 (1977) 129–135.
695 [https://doi.org/10.1175/1520-0450\(1977\)016<0129:EEOUEO>2.0.CO;2](https://doi.org/10.1175/1520-0450(1977)016<0129:EEOUEO>2.0.CO;2).
- 696 [39] I.D. Stewart, A systematic review and scientific critique of methodology in modern urban
697 heat island literature, *Int. J. Climatol*. 31 (2011) 200–217.
698 <https://doi.org/10.1002/joc.2141>.
- 699 [40] G. Pigeon, A. Lemonsu, N. Long, J. Barrié, V. Masson, P. Durand, Urban Thermodynamic
700 Island in a Coastal City Analysed from an Optimized Surface Network, *Boundary-Layer*
701 *Meteorol*. 120 (2006) 315–351. <https://doi.org/10.1007/s10546-006-9050-z>.

- 702 [41] M. Kottek, J. Grieser, C. Beck, B. Rudolf, F. Rubel, World Map of the Köppen-Geiger
703 climate classification updated, *Meteorologische Zeitschrift*. (2006) 259–263.
704 <https://doi.org/10.1127/0941-2948/2006/0130>.
- 705 [42] N.G.R. Perera, R. Emmanuel, A “Local Climate Zone” based approach to urban planning
706 in Colombo, Sri Lanka, *Urban Climate*. 23 (2018) 188–203.
707 <https://doi.org/10.1016/j.uclim.2016.11.006>.
- 708 [43] B. Bechtel, P.J. Alexander, J. Böhner, J. Ching, O. Conrad, J. Feddema, G. Mills, L. See, I.
709 Stewart, Mapping Local Climate Zones for a Worldwide Database of the Form and
710 Function of Cities, *ISPRS International Journal of Geo-Information*. 4 (2015) 199–219.
711 <https://doi.org/10.3390/ijgi4010199>.
- 712 [44] T. Gardes, R. Schoetter, J. Hidalgo, N. Long, E. Marquès, V. Masson, Statistical prediction
713 of the nocturnal urban heat island intensity based on urban morphology and
714 geographical factors - An investigation based on numerical model results for a large
715 ensemble of French cities, *Science of The Total Environment*. 737 (2020) 139253.
716 <https://doi.org/10.1016/j.scitotenv.2020.139253>.
- 717 [45] N. Long, T. Gardes, J. Hidalgo, V. Masson, R. Schoetter, Influence of the urban
718 morphology on the urban heat island intensity: an approach based on the Local Climate
719 Zone classification, *PeerJ Inc.*, 2018. <https://doi.org/10.7287/peerj.preprints.27208v1>.
- 720 [46] Y. Richard, J. Emery, J. Dudek, J. Pergaud, C. Chateau-Smith, S. Zito, M. Rega, T. Vairet, T.
721 Castel, T. Thévenin, B. Pohl, How relevant are local climate zones and urban climate
722 zones for urban climate research? Dijon (France) as a case study, *Urban Climate*. 26
723 (2018) 258–274. <https://doi.org/10.1016/j.uclim.2018.10.002>.
- 724 [47] T. Houet, G. Pigeon, Mapping urban climate zones and quantifying climate behaviors -
725 An application on Toulouse urban area (France), *Environmental Pollution*. 159 (2011)
726 2180–2192. <https://doi.org/10.1016/j.envpol.2010.12.027>.
- 727 [48] T.R. Oke, INSTRUMENTS AND OBSERVING METHODS REPORT No. 8, (n.d.) 51.
- 728 [49] OpenStreetMap, OpenStreetMap. (n.d.). <https://www.openstreetmap.org/copyright>
729 (accessed June 8, 2021).
- 730 [50] N. Haala, C. Brenner, Extraction of buildings and trees in urban environments, *ISPRS*
731 *Journal of Photogrammetry and Remote Sensing*. 54 (1999) 130–137.
732 [https://doi.org/10.1016/S0924-2716\(99\)00010-6](https://doi.org/10.1016/S0924-2716(99)00010-6).
- 733 [51] G. Pigeon, D. Legain, P. Durand, V. Masson, Anthropogenic heat release in an old
734 European agglomeration (Toulouse, France), *International Journal of Climatology*. 27
735 (2007) 1969–1981. <https://doi.org/10.1002/joc.1530>.
- 736 [52] D.J. Sailor, A review of methods for estimating anthropogenic heat and moisture
737 emissions in the urban environment, *International Journal of Climatology*. 31 (2011)
738 189–199. <https://doi.org/10.1002/joc.2106>.
- 739 [53] I.D. Stewart, T.R. Oke, Local Climate Zones for Urban Temperature Studies, *Bull. Amer.*
740 *Meteor. Soc.* 93 (2012) 1879–1900. <https://doi.org/10.1175/BAMS-D-11-00019.1>.
- 741 [54] F. Leconte, J. Bouyer, R. Claverie, M. Pétrissans, Using Local Climate Zone scheme for UHI
742 assessment: Evaluation of the method using mobile measurements, *Building and*
743 *Environment*. 83 (2015) 39–49. <https://doi.org/10.1016/j.buildenv.2014.05.005>.
- 744 [55] W.F. Holmgren, C.W. Hansen, M.A. Mikofski, pvlib python: a python package for
745 modeling solar energy systems, *Journal of Open Source Software*. 3 (2018) 884.
746 <https://doi.org/10.21105/joss.00884>.

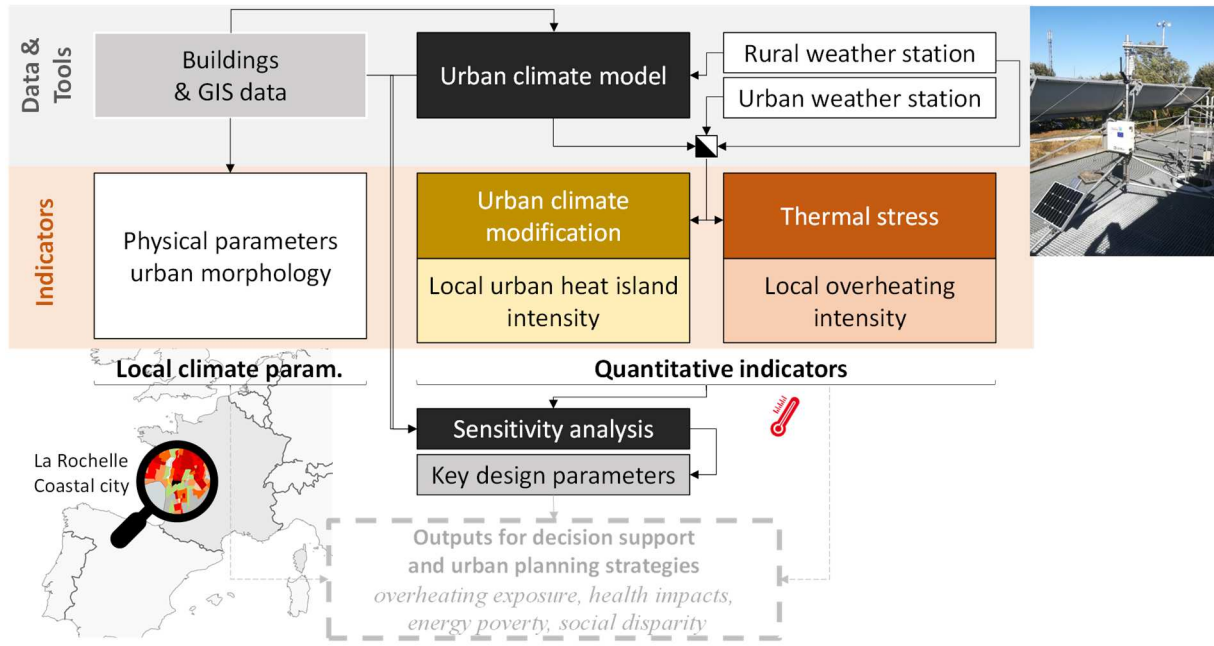
- 747 [56] E.L. Maxwell, A quasi-physical model for converting hourly global horizontal to direct
748 normal insolation, Solar Energy Research Inst., Golden, CO (USA), 1987.
749 <https://www.osti.gov/biblio/5987868> (accessed March 3, 2020).
- 750 [57] B.C. Rhodes, PyEphem: Astronomical Ephemeris for Python, Astrophysics Source Code
751 Library, Record Ascl:1112.014. (2011) ascl:1112.014.
- 752 [58] B. Bueno, A. Nakano, L. Norford, Urban weather generator: a method to predict
753 neighborhood-specific urban temperatures for use in building energy simulations, (n.d.)
754 6.
- 755 [59] O. US EPA, Measuring Heat Islands, US EPA. (2014).
756 <https://www.epa.gov/heatislands/measuring-heat-islands> (accessed July 12, 2021).
- 757 [60] ADEME, Urban overheating diagnostic - Diagnostic de la surchauffe urbaine, ADEME,
758 2017. [https://www.adaptation-changement-climatique.fr/centre-ressources/diagnostic-](https://www.adaptation-changement-climatique.fr/centre-ressources/diagnostic-la-surchauffe-urbaine)
759 [la-surchauffe-urbaine](https://www.adaptation-changement-climatique.fr/centre-ressources/diagnostic-la-surchauffe-urbaine).
- 760 [61] A. Martilli, E.S. Krayenhoff, N. Nazarian, Is the Urban Heat Island intensity relevant for
761 heat mitigation studies?, Urban Climate. 31 (2020) 100541.
762 <https://doi.org/10.1016/j.uclim.2019.100541>.
- 763 [62] N. Schwarz, S. Lautenbach, R. Seppelt, Exploring indicators for quantifying surface urban
764 heat islands of European cities with MODIS land surface temperatures, Remote Sensing
765 of Environment. 115 (2011) 3175–3186. <https://doi.org/10.1016/j.rse.2011.07.003>.
- 766 [63] N. Magee, G. Wendler, J. Curtis, The Urban Heat Island Effect at Fairbanks, Alaska,
767 Theoretical and Applied Climatology. 64 (1999) 39–47.
768 <https://doi.org/10.1007/s007040050109>.
- 769 [64] R.A. Memon, D.Y.C. Leung, C.-H. Liu, An investigation of urban heat island intensity
770 (UHII) as an indicator of urban heating, Atmospheric Research. 94 (2009) 491–500.
771 <https://doi.org/10.1016/j.atmosres.2009.07.006>.
- 772 [65] J. Martin-Vide, P. Sarricolea, M.C. Moreno-García, On the definition of urban heat island
773 intensity: the “rural” reference, Front. Earth Sci. 3 (2015).
774 <https://doi.org/10.3389/feart.2015.00024>.
- 775 [66] T.W. Hawkins, A.J. Brazel, W.L. Stefanov, W. Bigler, E.M. Saffell, The Role of Rural
776 Variability in Urban Heat Island Determination for Phoenix, Arizona, Journal of Applied
777 Meteorology and Climatology. 43 (2004) 476–486. [https://doi.org/10.1175/1520-](https://doi.org/10.1175/1520-0450(2004)043<0476:TRORVI>2.0.CO;2)
778 [0450\(2004\)043<0476:TRORVI>2.0.CO;2](https://doi.org/10.1175/1520-0450(2004)043<0476:TRORVI>2.0.CO;2).
- 779 [67] J. Vogel, A. Afshari, Comparison of urban heat island intensity estimation methods using
780 urbanized WRF in Berlin, Germany, (2020) 25.
- 781 [68] M. Kolokotroni, Y. Zhang, R. Giridharan, Heating and cooling degree day prediction
782 within the London urban heat island area, Building Services Engineering Research and
783 Technology. 30 (2009) 183–202. <https://doi.org/10.1177/0143624409104733>.
- 784 [69] B. à É.P. et R. Carbone, Projet de documents méthode pour la Réglementation
785 environnementale 2020 (RE2020), (2020). [http://www-maj.batiment-](http://www-maj.batiment-energiecarbone.e2.rie.gouv.fr/projet-de-documents-methode-pour-la-reglementation-a126.html)
786 [energiecarbone.e2.rie.gouv.fr/projet-de-documents-methode-pour-la-reglementation-](http://www-maj.batiment-energiecarbone.e2.rie.gouv.fr/projet-de-documents-methode-pour-la-reglementation-a126.html)
787 [a126.html](http://www-maj.batiment-energiecarbone.e2.rie.gouv.fr/projet-de-documents-methode-pour-la-reglementation-a126.html) (accessed June 8, 2021).
- 788 [70] M.D. Morris, Factorial Sampling Plans for Preliminary Computational Experiments,
789 Technometrics. 33 (1991) 161–174. <https://doi.org/10.1080/00401706.1991.10484804>.
- 790 [71] A.-T. Nguyen, S. Reiter, A performance comparison of sensitivity analysis methods for
791 building energy models, Build. Simul. 8 (2015) 651–664. [https://doi.org/10.1007/s12273-](https://doi.org/10.1007/s12273-015-0245-4)
792 [015-0245-4](https://doi.org/10.1007/s12273-015-0245-4).

- 793 [72] W. Tian, A review of sensitivity analysis methods in building energy analysis, *Renewable*
794 *and Sustainable Energy Reviews*. 20 (2013) 411–419.
795 <https://doi.org/10.1016/j.rser.2012.12.014>.
- 796 [73] V. Corrado, H.E. Mechri, Uncertainty and Sensitivity Analysis for Building Energy Rating,
797 *Journal of Building Physics*. 33 (2009) 125–156.
798 <https://doi.org/10.1177/1744259109104884>.
- 799 [74] L. Bande, A. Afshari, D. Al Masri, M. Jha, L. Norford, A. Tsoupos, P. Marpu, Y. Pasha, P.
800 Armstrong, Validation of UWG and ENVI-Met Models in an Abu Dhabi District, Based on
801 Site Measurements, *Sustainability*. 11 (2019) 4378. <https://doi.org/10.3390/su11164378>.
- 802 [75] M. Moradi, B. Dyer, A. Nazem, M.K. Nambiar, M.R. Nahian, B. Bueno, C. Mackey, S.
803 Vasanthakumar, N. Nazarian, E.S. Krayenhoff, L.K. Norford, A.A. Aliabadi, The Vertical City
804 Weather Generator (VCWG v1.3.2), *Geoscientific Model Development*. 14 (2021) 961–
805 984. <https://doi.org/10.5194/gmd-14-961-2021>.
- 806 [76] H.S. Khan, R. Paolini, M. Santamouris, P. Caccetta, Exploring the Synergies between
807 Urban Overheating and Heatwaves (HWs) in Western Sydney, *Energies*. 13 (2020) 470.
808 <https://doi.org/10.3390/en13020470>.
- 809 [77] T. Hong, Y. Chen, X. Luo, N. Luo, S.H. Lee, Ten questions on urban building energy
810 modeling, *Building and Environment*. 168 (2020) 106508.
811 <https://doi.org/10.1016/j.buildenv.2019.106508>.

812

813

1 Graphical abstract



2